Nature Methods

Ultra-bright Photoactivatable Fluorophores Created by Reductive Caging

Joshua C. Vaughan, Shu Jia, Xiaowei Zhuang

Supplementary Figure 1	Reductive caging and photoactivation of Atto 488, Cy3, Alexa 647, and Cy5.5.
Supplementary Figure 2	Single-molecule characterization of the photon yield and localization precision of Atto 488, Cy3, Cy3B, Alexa 647, and Cy5.5.
Supplementary Figure 3	Excitation intensity dependence of the switching properties of reductively caged fluorophores, Atto 488, Cy3B, and Alexa 647.
Supplementary Figure 4	Simulation of the transverse profile of a microtubule.
Supplementary Figure 5	Conventional fluorescence and STORM images of M13 bacteriophage viruses directly labeled with Cy3B
Supplementary Figure 6	Transmission electron microscopy images of microtubules and M13 bacteriophage viruses with and without treatment by sodium borohydride.
Supplementary Figure 7	Reduction kinetics for Cy3B in the presence of $NaBH_4$.
Supplementary Figure 8	Assessment of the rotational freedom of Atto 488, Cy3, Cy3B, Alexa 647, and Cy5.5 by defocus imaging.
Supplementary Figure 9	Quantification of defocusing-induced localization errors for Cy3B and Alexa 647 in comparison with fluorescent beads and polymer-embedded DiI molecules.
Supplementary Note	Discussion of dipole orientation effects on localization precision.
Supplementary Protocol	Detailed protocol for preparation and imaging of *in vitro* microtubules.

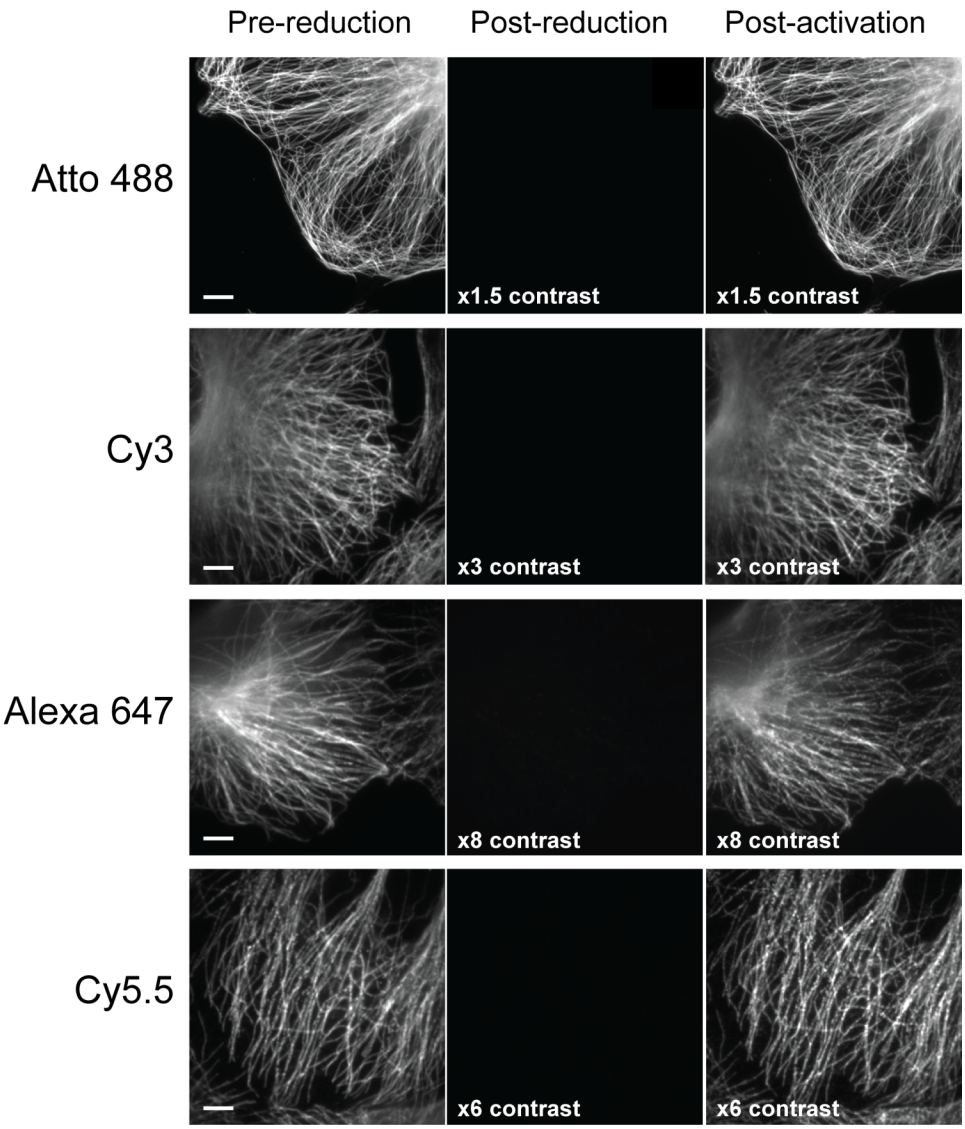

Supplementary Figure 1. Reductive caging and photoactivation of Atto 488, Cy3, Alexa 647, and Cy5.5. BS-C-1 cells were immunostained for microtubules with Alexa 488, Cy3, Alexa 647, or Cy5.5. Fluorescence images were recorded prior to reduction with sodium borohydride (left column), just after reduction and washing with PBS (middle column), and after re-activation with ultraviolet light (right column). The image contrast in the post-activation images (and post-reduction images) was multiplied by the factors indicated compared to the pre-reduction case. Scale bar, 5 μm.

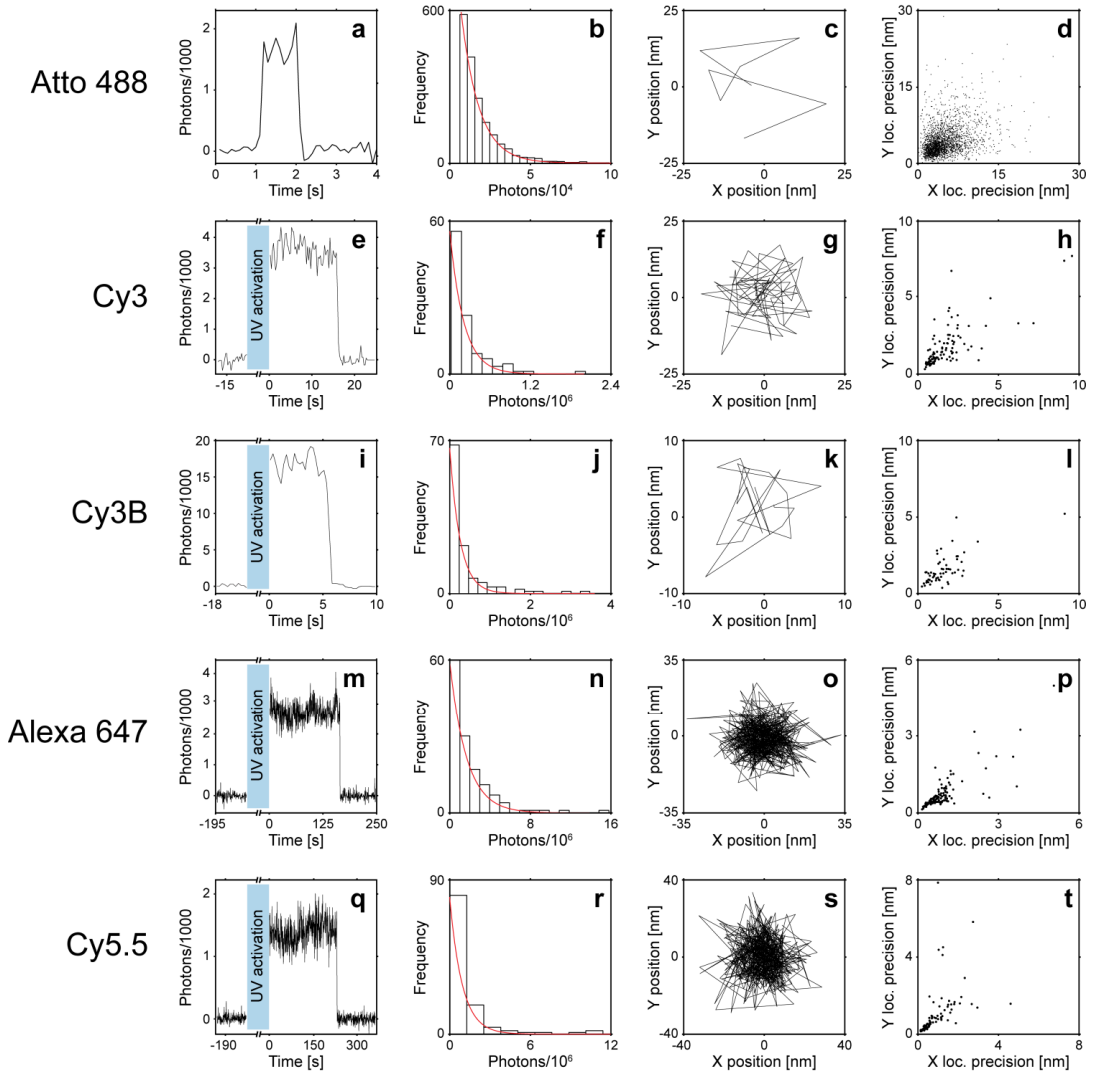

Supplementary Figure 2. Single-molecule characterization of the photon yield and localization precision of Atto 488, Cy3, Cy3B, Alexa 647, and Cy5.5. Dye-labeled antibodies were adsorbed to coverglass, reduced with sodium borohydride, and imaged as the molecules returned to the bright state. Example single-molecule fluorescence time traces are shown in (**a**, **e**, **i**, **m**, **q**) for each dye. For Cy3, Cy3B, Alexa 647, and Cy5.5, dyes were not illuminated with their respective excitation lasers (561 nm for Cy3 and Cy3B, and 647 nm for Alexa 647 and Cy5.5) during activation by 405 nm light (indicated by the blue boxes in **e**, **i**, **m**, **q**). For Atto 488 (**a**), molecules were activated and imaged with 488 nm light without 405 nm illumination. The fluorescence signal was recorded until the molecules were switched off or photobleached. The low density of adsorbed antibodies, low dye-to-protein ratio, and single-step photobleaching ensured that the fluorescence signals originated from single dye molecules. The distribution of photons detected per molecule before switching off (**b**, **f**, **j**, **n**, **r**) was fitted to an exponential distribution (red lines) to determine the mean number of detected photons, as reported in **Fig. 1c**. Each molecule was imaged for multiple frames

before switching off (**c**, **g**, **k**, **o**, **s**). The localizations recorded in all frames were used to determine the mean value and the standard error of the mean (SEM), the latter of which represents the localization uncertainty (precision) for the molecule when all detected photons are taken into account. For each dye type, the localization precisions (loc. precision) determined from many (≥100) molecules is presented as a scatter plot in (**d**, **h**, **l**, **p**, **t**) and the average localization precision value is presented in **Fig. 1d** (left axis). Note that for these measurements, the continuous fluorescence emission from single molecules was deliberately divided into many frames to allow the determination of the localization uncertainty for each molecule. Consequently, the localization spread (the standard deviation) from frame to frame was relatively large for each molecule since the number of photons detected per frame was relatively low. Nonetheless, the small standard error of the mean (standard deviation divided by the square root of the number of frames) represents how precisely the average localization of the molecule was determined during its entire emission period when all detected photons were taken into account. Rebinning the trajectories into substantially fewer points (i.e., combining 16 frames into one) did not change the standard errors appreciably, indicating that our low standard errors of the mean are not an artifact of dividing the total photons into a very large number of frames.

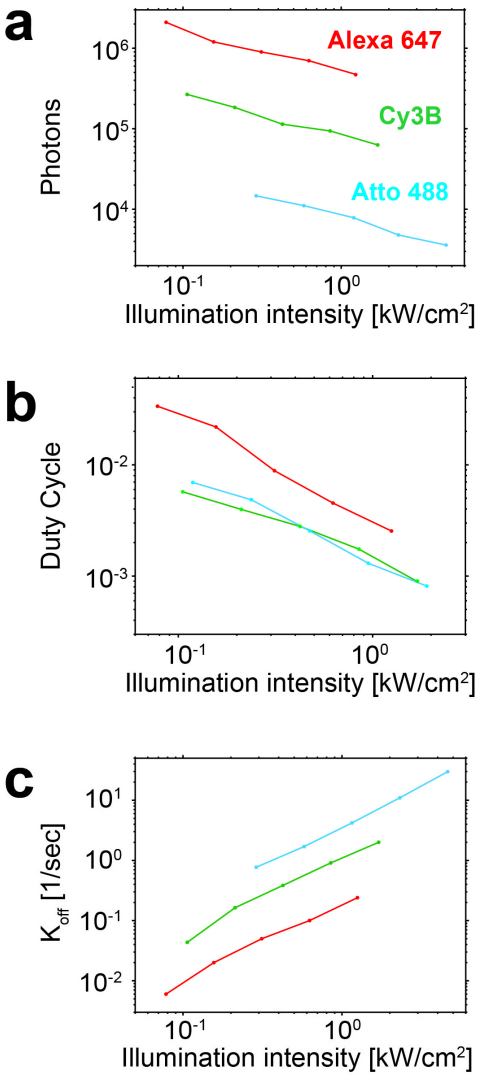

Supplementary Figure 3. Excitation intensity dependence of the switching properties of reductively caged Atto 488, Cy3B, and Alexa 647. (**a**) The number of photons detected per activation event at different illumination intensities. (**b**) The on-off duty cycle (defined as the fraction of time that the molecules spend in the on state) at different illumination intensities. (**c**) The switching-off rate constants k_{off} as a function of the illumination intensity. The spontaneous (thermal) activation rates for all reduced fluorophores in the absence of illumination were very low, on the order of (1-10) × 10^{-4} min^{-1}. Upon illumination with 405 nm light (~0.2 kW/cm^2), the activation rates were increased by 2-5 orders of magnitude.

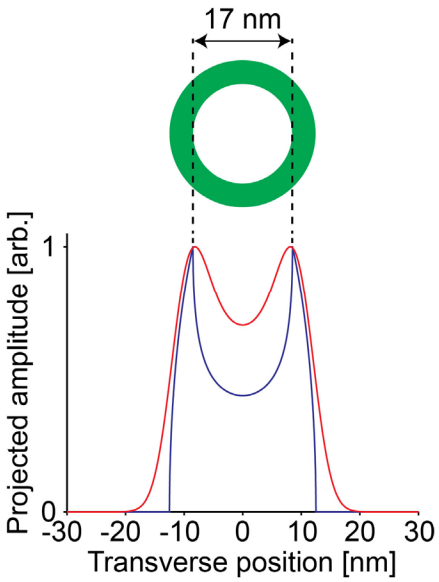

Supplementary Figure 4. Simulation of the transverse profile of a microtubule. Structural studies on microtubules have established that microtubule walls contain regular arrays of deep corrugations and fenestrations[1]. It is also established that microtubules are highly porous and permit various molecules with sizes comparable to Cy3B to enter their lumen[1]. It is thus likely that Cy3B is able to efficiently access both outer and inner surfaces of the microtubule, as well as its corrugations and fenestrations, such that the entire thickness of the microtubule wall is effectively labeled. On this basis, we model microtubules as a uniform hollow cylinder with 25 nm outer diameter and 17 nm inner diameter[1]. The blue curve shows the simulated transverse profile of the probe density assuming that the microtubule is uniformly labeled, while the red curve shows the profile after convolution with a Gaussian of 6 nm FWHM to simulate blurring due to the ~6 nm image resolution.

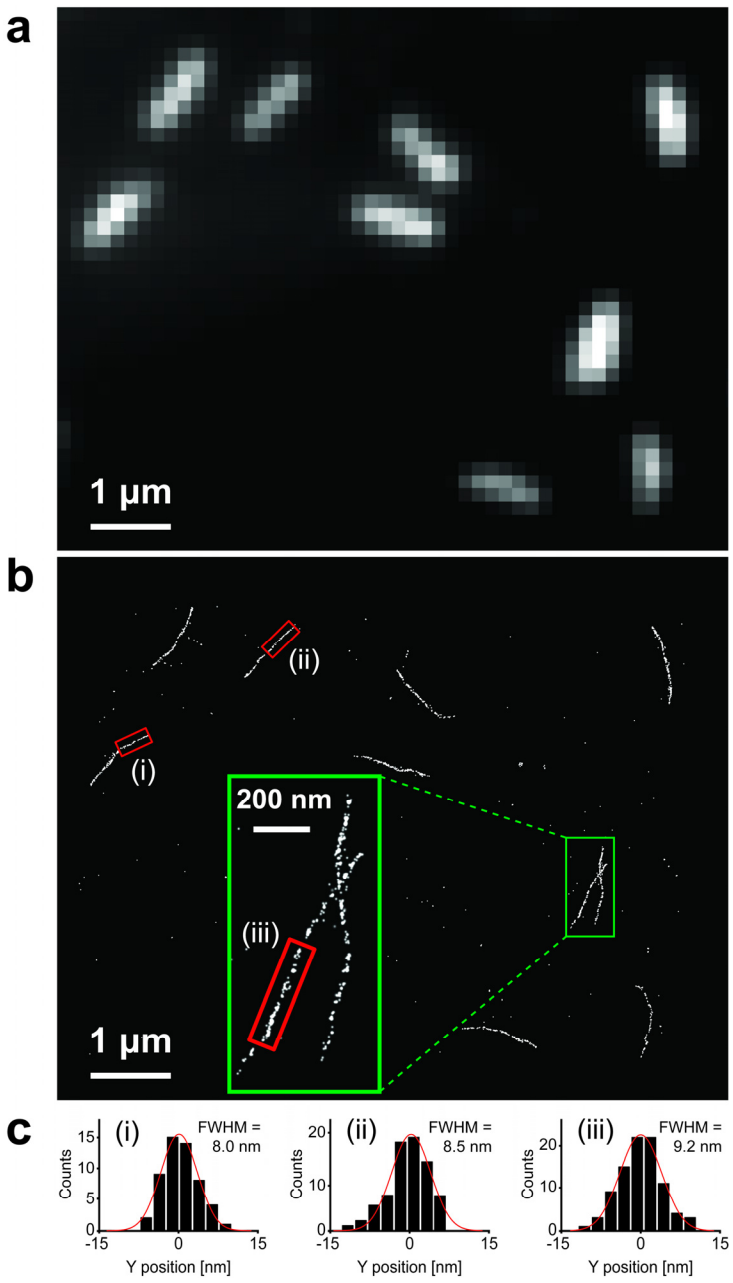

Supplementary Figure 5. Conventional fluorescence and STORM images of M13 bacteriophage viruses directly labeled with Cy3B. (**a**) Conventional fluorescence image. (**b**) STORM image obtained after reduction with sodium borohydride and subsequent photoactivation for the same field of view. (**c**) Transverse profiles of the regions of the viruses in the corresponding red boxes in (**b**). The red curves are nonlinear least-squares fits of the distributions to a Gaussian function, allowing the FWHM of the virus particles to be derived. Analysis of a panel of 12 independent virus particles revealed a mean width of 9.0 ± 0.7 nm, which is in good agreement with the known 7 nm diameter of the virus and the expected blurring due to the ~6 nm obtainable resolution. The average separation between localizations was 6-7 nm for these images.

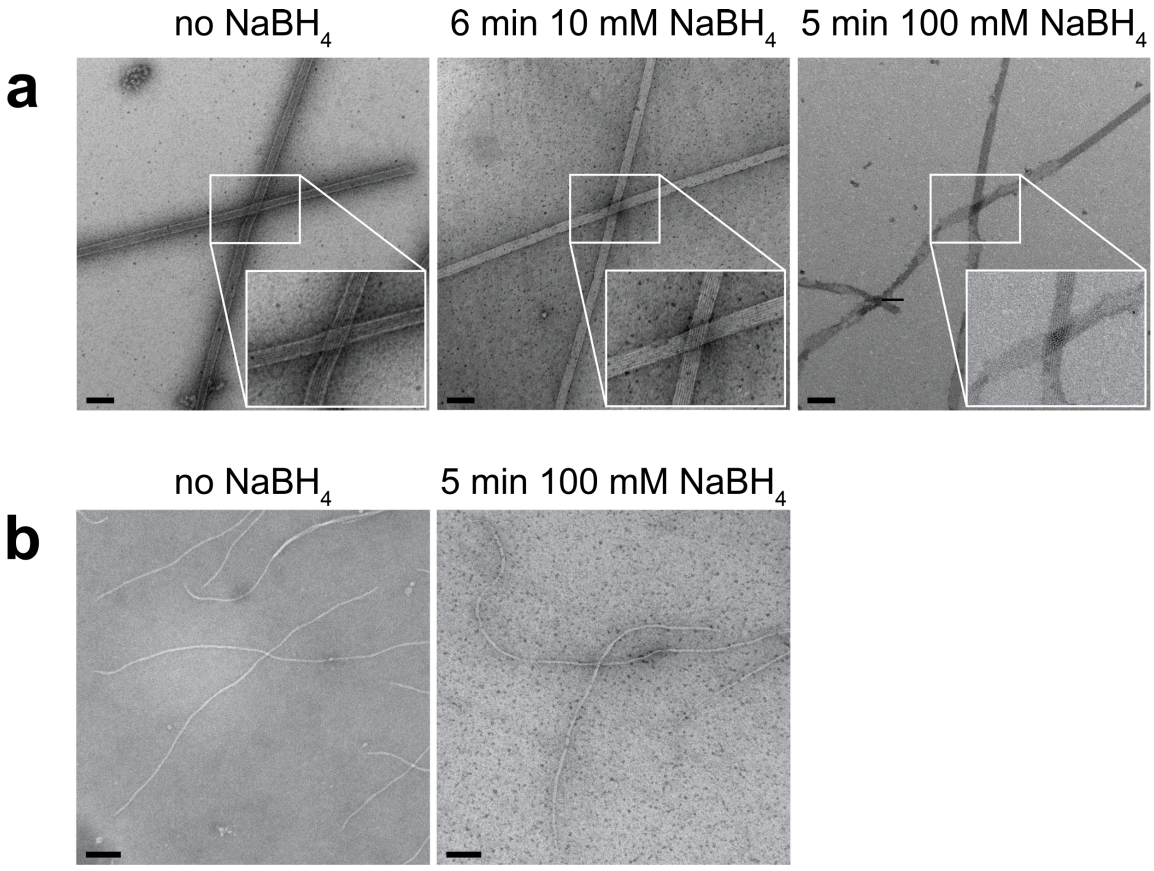

Supplementary Figure 6. Transmission electron microscopy images of microtubules (**a**) and M13 bacteriophage viruses (**b**) with and without treatment by sodium borohydride ($NaBH_4$). Zoom-in images of microtubules in the boxed regions are shown in the lower right corners of the panels in (**a**). The ultrastructure of fixed microtubules is typically not perturbed by 6 min, 10 mM $NaBH_4$ treatment, although stronger treatments, such as 5 min 100 mM $NaBH_4$ (right panel) or much longer reductions with 10 mM $NaBH_4$ (not shown) may degrade microtubules. In contrast, the (unfixed) M13 particles appear unchanged after 5 min, 100 mM $NaBH_4$ treatment. STORM images of microtubules (Fig. 3) were taken after 4 min, 10 mM $NaBH_4$ treatment, whereas those of M13 (Supplementary Fig. 5) were taken after 5 min, 30 mM $NaBH_4$ treatment. Scale bars 100 nm. Insets in (**a**) have been magnified twofold.

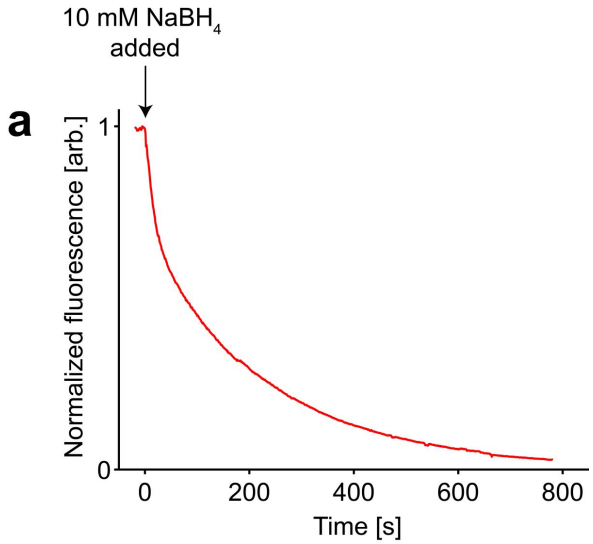

Supplementary Figure 7. Reduction kinetics for Cy3B in the presence of $NaBH_4$. Cy3B-labeled microtubules were adsorbed to coverglass, fixed, incubated with water, and imaged under the microscope. At time t = 0 an aqueous solution of $NaBH_4$was added to achieve a final $NaBH_4$ concentration of 10 mM. The observed fluorescence from the microtubules is displayed as a function of time. In STORM imaging experiments, we typically treat the sample with 10 mM $NaBH_4$ for ~4 min (**Fig. 3**), at which point ~75% of the dye molecules were reduced. The remaining non-reduced molecules can be pre-bleached before STORM imaging to avoid excessive fluorescence background. Note that higher concentrations of $NaBH_4$ reduced Cy3B at higher rates, with an approximately linear dependence of reduction rate on $NaBH_4$ concentration (data not shown).

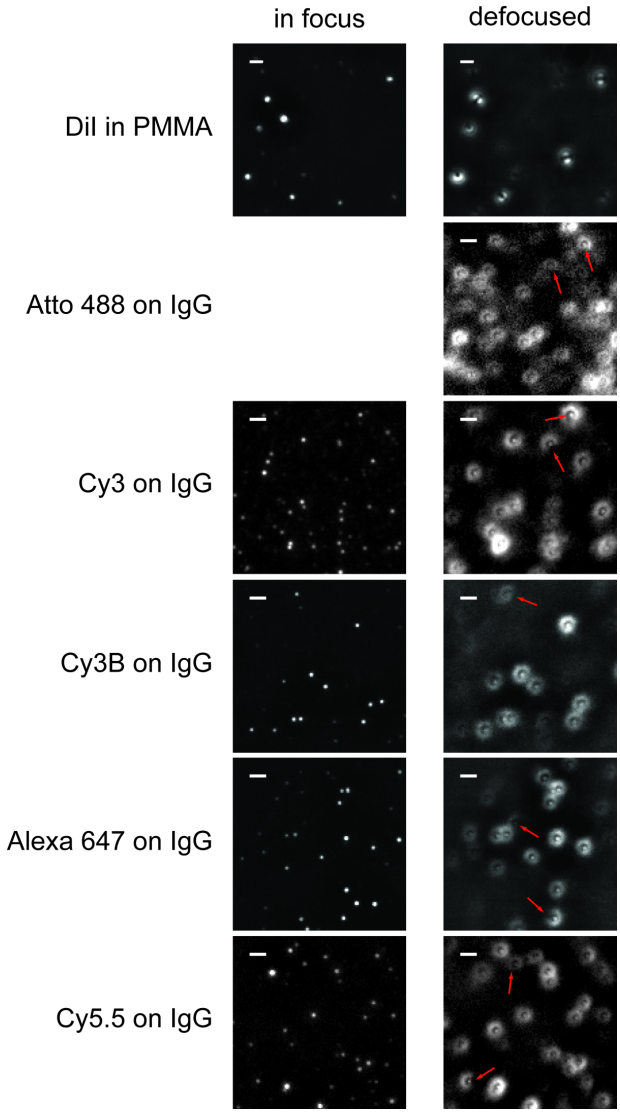

Supplementary Figure 8. Assessment of the rotational freedom of Atto 488, Cy3, Cy3B, Alexa 647, and Cy5.5 by defocus imaging. In-focus and defocused images of single dye molecules. The defocused images were taken with the molecules ~850 nm from the focal plane. Atto 488, Cy3, Cy3B, Alexa 647, Cy5.5 were conjugated to antibodies and adsorbed on coverglass. DiI fluorophores embedded in poly(methyl methacrylate) (PMMA) were imaged for comparison. DiI molecules in PMMA are rotationally constrained and show highly asymmetric patterns when imaged out of focus[2,3]. In contrast, dyes conjugated to antibodies showed much more symmetric emission patterns in the defocused images, although a small fraction (~20%) of the molecules showed some amount of asymmetry (examples shown with red arrows). Only a defocused image is provided for Atto 488, because the relatively rapid bleaching of this dye made it difficult to obtain both focused and defocused images of the same field of view with high signal-to-noise ratio. Scale bars: 1 μm.

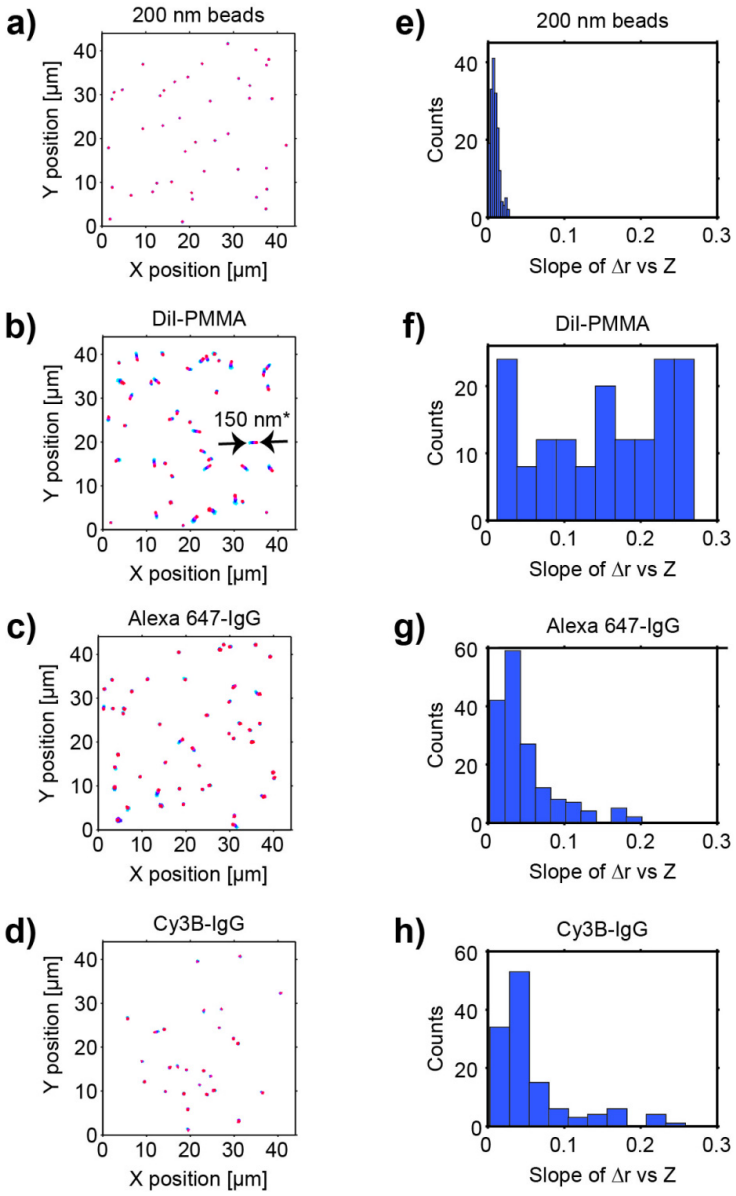

Supplementary Figure 9. Quantification of defocus-induced localization errors for Cy3B and Alexa 647 in comparison with fluorescent beads and polymer-embedded DiI molecules. Various fluorescent dye samples were imaged (**a**)-(**d**) and the lateral (x, y) positions of the molecules were tracked as the microscope focal plane was scanned over a range 700 nm (i.e. samples were scanned from 350 nm below the focal plane to 350 nm above the focal plane). The slope of the average lateral displacement of the dye molecule as a function of the defocus distance was calculated for each trajectory and the histogram of the slopes were plotted in (**e**)-(**h**). Fluorescent beads showed essentially no lateral motion due to defocusing (mean slope = 0.009, meaning that a 0.9 nm lateral movement was induced by 100 nm movement of the focal plane). In contrast, DiI molecules embedded in PMMA showed strong linear shifts as a function of defocus (mean slope = 0.15). Alexa 647 and Cy3B molecules conjugated to antibodies adsorbed

to glass showed substantially smaller lateral displacements (mean slopes = 0.049 and 0.058, respectively), indicating that the fluorophores are much freer to rotate than the rotationally constrained DiI in PMMA. *Note that the lateral displacements within individual trajectories in (**a**)-(**d**) have been magnified tenfold for the sake of clarity.

Supplementary Note: Discussion of dye orientation effects on localization precision.

Although single fluorophores are often treated as isotropic point sources of light, they are in fact dipole emitters. Because of this, in situations when the orientation of the fluorophore is not freely rotating on the time scale of the measurement, the centroid position of its image may deviate from the molecule's true position[2-4]. These fixed-dipole errors have been theoretically and experimentally shown to be largest for defocused images[2,3], although simulations[3] have also shown that smaller, in-focus errors may also occur.

To estimate the dipole orientation effects, we performed two sets of experiments. In the first set of measurements (**Supplementary Fig. 8**), we used defocused images of single molecules to assess the extent to which dye molecules are rotationally constrained. The dye DiI was embedded in a polymer and used to simulate a fluorophore without rotational freedom. The images of these rotationally constrained DiI molecules showed a variety of crescent and dumbbell shapes that deviated dramatically from the Airy-disc like pattern expected for an isotropic or freely rotating emitter. In contrast, only a small fraction (<20%) of the dye-labeled antibodies adsorbed to coverglass showed appreciable anisotropic effects. Moreover, the defocused images of this small fraction of molecules were much more isotropic than those observed for the rotationally constrained DiI. We also note that even the in-focus images from embedded DiI sometimes showed donut shapes, as previously reported[5], but such shapes were not observed for the in-focus images of dye-labeled antibodies (data not shown). These observations suggest that that the dye-labeled proteins used in our studies are much more freely rotating than truly fixed dipoles.

In the second set of measurements (**Supplementary Fig. 9**), we evaluated the magnitude of localization errors induced by defocusing of fixed dipoles by performing z-scans of embedded DiI molecules and dye-labeled antibodies, and comparing these results with those obtained from isotropic fluorescent beads. We found that embedded DiI molecules typically showed linear defocus trajectories with an average slope of ~0.15, meaning that for a molecule placed 100 nm from the focal plane, the centroid position of its image deviates from its true position by ~15 nm. The defocusing trajectories of beads showed much smaller slopes (<0.01), while those of Alexa 647 or Cy3B dye molecules conjugated to antibodies showed intermediate slopes (0.05-0.06). In the case of thin (<50 nm), well-focused samples, such as microtubules in **Fig. 3** and bacteriophage in **Supplementary Fig. 5**, the possible defocusing-induced localization error (less than 2.5-3 nm) was therefore small compared to the STORM image resolution that we reported for these samples (~6 nm). It should be noted that these defocus-induced localization errors are somewhat larger than the best image resolution potentially obtainable from Alexa 647 and Cy5.5 (1-2 nm). Thus, additional efforts to reduce or correct for the dye orientation effect may be required to fully capitalize on the large photon yields of these dyes for obtaining image resolution at the 1-2 nm scale.

Beyond the error caused by defocused dipoles, well-focused images of fixed dipoles may also exhibit localization errors. Through a systematic series of simulations, Enderlein et al.[4] showed that the effects are worse for dim fluorophores and for dipoles at certain zenith angles. For fixed dipoles with the level of photon yields shown in this work, ~10^4-10^6 photons, the in-focus localization errors would be expected to be ~4 nm or less[4]. For dyes that suffer only partial or occasional hindrance of rotation as shown for our dye-labeled proteins, the effects should be even smaller. Enderlein et al. also suggest that use of water-immersion objectives and higher magnification should virtually eliminate in-focus fixed-dipole errors, provided that sufficiently many photons are observed per localization. Given that our photoactivatable, reduced fluorophores have high photon yields, it should be possible to further reduce the in-focus localization errors resulting from fixed-dipole effects when using a water-immersion objective lens and higher magnification. Additionally, the high photon yield should more than compensate for the lower collection efficiency and slightly larger point-spread function of water-immersion lenses—factors which typically favor use of high numerical aperture oil-immersion lenses for STORM.

Taken together, these results indicate that the dye molecules studied here behave more like isotropic emitters than fixed-dipoles, although some extent of hindered rotation was observed. The dipole-orientation induced localization errors for these dyes in well-focused samples are smaller than our reported STORM image resolution. Additional reduction or correction for dipole induced errors may be required for studies at 1-2 nm scales or when imaging thicker samples. The dye orientation effects may be further reduced by utilizing passivated surfaces for to minimize surface-fluorophore interactions, as well as by using water-immersion objectives and higher magnification imaging systems.

References

1. E. Nogales, M. Whittaker, R. A. Milligan et al., *Cell* **96**, 79-88 (1999).
2. A. P. Bartko and R. M. Dickson, *J. Phys. Chem. B* **103**, 11237-11241 (1999).
3. J. Engelhardt, J. Keller, P. Hoyer, M. Reuss, T. Staudt, S.W. Hell, *Nano. Lett.* **11**, 209-213 (2011).
4. J. Enderlein, E. Toprak, and P. R. Selvin, *Opt. Express* **14**, 8111-8120 (2006).
5. R. M. Dickson, D. J. Norris, and W. E. Moerner, *Phys. Rev. Lett.* **81**, 5322-5325 (1998).

Supplementary Protocol: Step-by-step protocol for *in vitro* microtubule sample preparation.

1. **Reagents or materials to obtain or prepare**
    a. 1 mg aliquot of purified tubulin (T240; Cytoskeleton)
    b. GTP aliquot (BST06; Cytoskeleton)
    c. Paclitaxel aliquot (TXD01; Cytoskeleton)
    d. 10x concentration of aqueous PEM buffer (1 M PIPES buffer pH 7.0, 10 mM EGTA, 10 mM $MgCl_2$). A stock of 10x PEM may be prepared and stored for months if protected from light.
    e. Anhydrous DMSO
    f. Cy3B-NHS (GE Healthcare)
    g. N-[3-(Trimethoxysilyl)propyl]ethylenediamine (104884; Sigma)
    h. Glutaraldehyde
    i. Sodium borohydride
    j. 1 μm diameter nonfluorescent beads (C37483; Invitrogen)
    k. LabTek 8-well chambers (154534; Nunc) or similar sample holder with open well above coverglass for easy buffer exchange.
2. **General notes**
    a. Use ultrapure water (e.g. MilliQ) whenever water or aqueous solutions are used.
    b. Use freshly prepared solutions of 20 μM paclitaxel (e.g., PEM-P, see below) for all steps involving paclitaxel. Paclitaxel at a concentration of 20 μM tends to precipitate within ~30 min.
    c. Use blunt 200 μL pipette tips (e.g. cut with scissors) for mixing or pipetting of microtubules with minimal shear-flow damage.
3. **Microtubule growth**
    a. Freshly prepare 100 mM aqueous GTP stock and store on ice.
    b. Freshly prepare 2 mM paclitaxel stock in DMSO and store at room temperature (~22 °C).
    c. Prepare tubulin growth buffer consisting of PEM (100 mM PIPES pH 7, 1 mM EGTA, 1 mM $MgCl_2$) + 10% glycerol + 1 mM GTP by mixing 197.5 μL water, 25 μL 10x PEM, 25 μL glycerol, and 2.5 μL 100 mM GTP stock.
    d. Prechill 1 mg tubulin aliquot and tubulin growth buffer by incubating both on ice.
    e. Add 250 μL tubulin growth buffer to 1 mg tubulin aliquot and mix thoroughly until tubulin is fully dissolved. Avoid generating bubbles. At this point, aliquots of dissolved tubulin may be snap-frozen in liquid nitrogen and stored at -80 °C, to be thawed when ready and resume the growth protocol.
    f. Incubate tubulin solution at 37 °C for 20 min to polymerize microtubules.

g. Stabilize microtubules by adding 2.5 µL of 2 mM paclitaxel to microtubule solution for a final concentration of ~20 µM paclitaxel. Mix by pipetting up and down using blunt 200 µL pipette tip.
h. Incubate microtubule-paclitaxel solution for 5 min at 37 °C, and then store microtubules at room temperature. Microtubules should be stable for a few days.

4. Microtubule labeling

a. Dissolve Cy3B-NHS in anhydrous DMSO to a concentration of 10 mg/mL. Cy3B-NHS DMSO stock may be stored frozen at -20 °C for weeks to months.
b. Add ~2 µL of 10 mg/mL Cy3B-NHS to 60 µL of paclitaxel-stabilized microtubules (~4 mg/mL) and mix well. Use blunt 100 µL pipette tips for mixing to minimize shear-flow damage to microtubules.
c. Incubate Cy3B-microtubule solution at room temperature for ~45 min while protected from light.
d. Extent of labeling may be characterized by recording UV-Vis absorption spectra of labeled microtubules and comparing the absorption peak at ~280 nm with that at ~560 nm. Typical ratios of the 280 nm / 560 nm absorption peaks were in the range 1:2 – 1:1.
e. The extent of labeling may be varied by adjusting the concentration of Cy3B-NHS and/or the duration of the labeling reaction.

5. Purification of labeled microtubules

a. Prepare 1 mL of centrifugation solution (PEM + 60% glycerol (v/v) + 20 µM paclitaxel) by mixing 600 µL glycerol, 290 µL water, 100 µL 10x PEM, and 10 µL of 2 mM paclitaxel.
b. Pipette 550 µL of centrifugation solution into small ultracentrifugation tube (e.g. Beckman catalog # 344090, compatible with SW55-Ti rotor when using adapter catalog # 356860).
c. Add the ~60 µL Cy3B-microtubule solution on top of the centrifugation solution.
d. Centrifuge Cy3B-microtubules for 2 hours at 300,000 g at 25 °C. Pinkish Cy3B-labeled microtubules should form a small pellet at the bottom of the tube, while free Cy3B or Cy3B-labeled tubulin heterodimers will remain at the top of the tube.
e. Discard supernatant, taking care to cleanly remove free Cy3B and Cy3B-labeled tubulin heterodimer without mixing them with the pellet.
f. Wash the pellet 3 times, each with ~100 µL fresh PEM-P (PEM + 20 µM paclitaxel). Use blunt, 200 µL tips for washes.
g. Resuspend the pellet in 50 µL fresh PEM-P. Use blunt 200 µL tips to start, but if resuspension is not complete, switch to more vigorous pipetting using a normal (non-blunt) 200 µL tip. Excess shear flow may lead to small microtubules and diffuse background from chopped up microtubule pieces. Store resuspended, labeled microtubules in the dark at room temperature for up to a day.

6. **Prepare 8-well chambers for microtubule and bead adsorption**
    a. Sonicate LabTek 8-well chamber for ~20 min in 1 M aqueous potassium hydroxide solution. The 8-well chambers conveniently fit into standard 50 mL conical tubes which may be filled with KOH and then immersed into a bath sonicator.
    b. Wash chamber extensively with water and allow to dry.
    c. Aminosilanize well surface by incubation with freshly prepared silanization solution (1% N-[3-(Trimethoxysilyl)propyl]-ethylenediamine, 5% acetic acid, and 94% methanol) for 20 min. ~200 µL silanization solution is sufficient per well.
    d. Wash extensively with water and allow to dry.
    e. Cleaned/aminosilanized chambers may be stored for many weeks before but should be stored while protected from dust.
7. **Adsorb microtubules and beads to 8-well chamber**
    a. Dilute Cy3B-labeled microtubules ~1:500 in fresh PEM-P along with a ~1:200 dilution of 1 µm diameter nonfluorescent beads.
    b. Incubate ~150 µL diluted Cy3B-labeled microtubules and beads for ~10 min in silanized LabTek 8-well chamber well.
    c. Wash well 3-6 times with fresh PEM-P to remove unbound microtubules and beads. For this step and all subsequent steps with the sample, only perform partial buffer exchanges (~80%) for washes or changing the solution such that at least ~100 µL liquid remains in each well. This avoids dragging the meniscus of the solution over the surface, which appeared to damage the microtubules.
    d. Repeat steps 7a-c if necessary to obtain the desired density of microtubules and beads.
    e. Fix microtubules with 1% glutaraldehyde in fresh PEM-P for ~20 min, followed by washing with fresh PEM-P. Fixed samples were stored at room temperature in the dark in PEM for up to 24 hours.
8. **Reduction of microtubules and imaging**
    a. Prepare imaging buffer consisting of 100 mM Tris at pH 8.0, 1 mM ascorbic acid with 1 mM methyl viologen, and the glucose oxidase/catalase based oxygen scavenging system (40 µg/mL catalase, and 5% (w/v) glucose, final concentrations).
    b. Reduce sample for ~5 min with aqueous 10 mM $NaBH_4$ prepared immediately before use, and then wash thoroughly with PBS.
    c. Change buffer to imaging buffer and record STORM image.